

Charge-two Weyl phonons with type-III dispersion

Guangqian Ding,^{1,*} Feng Zhou,^{2,*} Zeying Zhang,^{3,†} Zhi-Ming Yu^{1b,4}, and Xiaotian Wang^{1b,2,‡}

¹*School of Science, Chongqing University of Posts and Telecommunications, Chongqing 400065, China*

²*School of Physical Science and Technology, Southwest University, Chongqing 400715, China*

³*College of Science, Beijing University of Chemical Technology, Beijing 100029, China*

⁴*Key Lab of Advanced Optoelectronic Quantum Architecture and Measurement (MOE), Beijing Key Lab of Nanophotonics & Ultrafine Optoelectronic Systems, and School of Physics, Beijing Institute of Technology, Beijing 100081, China*



(Received 30 December 2021; revised 9 March 2022; accepted 15 April 2022; published 25 April 2022)

In recent years, charge-two Weyl point phonons (WPPs) have attracted increasing attention. Charge-two WPPs not only provide a new platform for realizing phonon-based unconventional Weyl points (WPs) but also help in realizing specific phonon-based transport behaviors. Herein, based on the first-principles calculations and symmetry analysis, we propose a realistic material with the $P3_121$ space group, BaZnO_2 , which has a charge-two WPP and two charge-one WPPs at high-symmetry points. These three unpaired WPPs form a unique triangular Weyl complex. Unlike previously reported material candidates with type-I or type-II charge-two WPPs, the proposed BaZnO_2 has a type-III charge-two WPP, which has a constant frequency surface that contains two electronlike or holelike states connected at the charge-two WP. BaZnO_2 can support double-helicoid phonon surface states that cover the entire (001) surface Brillouin zone. The clean type-III WPP, unique triangular Weyl complex, and clear and long surface states in BaZnO_2 suggest that it is an excellent platform for further research into the physics and applications of type-III charge-two WPPs. Furthermore, we pointed out that charge-two WPPs with type-III band dispersion may appear at high-symmetry points in space groups 75–80, 89–98, 143–146, 149–155, 168–173, 177–182, 196, 207–210. Besides trigonal BaZnO_2 , some material candidates, including tetragonal MgTiO_4 , trigonal Li_2GeF_6 , hexagonal CaSO_4 , and cubic $\text{Li}_{10}\text{B}_{14}\text{Cl}_2\text{O}_{25}$, are also shown to be the hosts of type-III charge-two WPPs.

DOI: [10.1103/PhysRevB.105.134303](https://doi.org/10.1103/PhysRevB.105.134303)

I. INTRODUCTION

In recent years, three-dimensional Weyl semimetals (WSMs) [1–3], which have discrete and finite degenerate points in the Brillouin zone (BZ), have attracted global attention and are believed to have ushered in a new era in the topological aspects of condensed-matter physics. Thus far, WSMs have been predicted in a large number of quantum materials [4–10], including $\text{Y}_2\text{Ir}_2\text{O}_7$ [4], TaAs [5–8], TaP [5], NbAs [5], NbP [5], HgCr_2Se_3 [9], and $\text{Hg}_{1-x-y}\text{Cd}_x\text{Mn}_y\text{Te}$ [10], and they also exhibit exotic physical phenomena, such as helical Fermi arcs [11], giant magneto-optical responses [12], chiral-anomaly-induced negative magnetoresistance [13], and the anomalous Hall effect [14–16]. Weyl points (WPs) in WSMs are typically divided into two types: conventional WPs, which have a chiral charge of ± 1 , and unconventional WPs [17–21], which have a chiral charge of ± 2 , ± 3 , or ± 4 . Conventional WPs are zero-dimensional twofold band degeneracies with a linear energy splitting along any direction in momentum space. WSMs with conventional WPs can be further divided into type-I [3,22] [see Figs. 1(a) and 1(d)], which respects Lorentz symmetry, and type-II [23,24], which

does not respect Lorentz symmetry [see Figs. 1(b) and 1(e)]. Unconventional WPs with chiral charges of ± 2 , ± 3 , and ± 4 are usually called charge-two (C-2), charge-three (C-3), and charge-four (C-4) WPs, respectively. C-2 and C-3 WPs have a linear dispersion along one direction and a quadratic energy splitting in the plane normal to the direction. C-4 WPs have a cubic dispersion along one direction and a quadratic energy splitting in the plane normal to the direction.

Figures 1(c) and 1(g)–1(i) depict some typical band structures of possible C-2 WPs in three-dimensional crystals. The WSMs with C-2 WPs are divided into four categories based on the crossing band slopes. Figure 1(c) shows the type-I C-2 WSMs with a pointlike Fermi surface, in which the holelike (h-like) and electronlike (e-like) states are separated [see Fig. 1(f)]. Figure 1(g) shows the type-II C-2 WSMs with overtilted Weyl cones, which have a Fermi surface that consists of both e-like and h-like states [see Fig. 1(j)]. Jin *et al.* [25] and Li *et al.* [26] recently proposed a new type of topological materials with type-III C-2 WPs. As shown in Figs. 1(h) and 1(i), the Fermi surface in the type-III C-2 WSMs contains two contacted e-like [see Fig. 1(k)] or h-like [see Fig. 1(l)] states. More interestingly, Jin *et al.* [25] proposed a family of ferromagnetic materials, $X_2\text{RhF}_6$ ($X = \text{K}, \text{Rb}, \text{Cs}$), with space group $P\bar{3}m1$, as type-III C-2 Weyl half metals, while Li *et al.* [26] proposed a nonmagnetic material with space group $I422$, $(\text{TaSe}_4)_2\text{I}$, which was synthesized 30 years ago, as a type-III C-2 WSM. However, the type-III C-2 WP in $(\text{TaSe}_4)_2\text{I}$

*These authors contributed equally to this work.

†zzy@mail.buct.edu.cn

‡xiaotianwang@swu.edu.cn

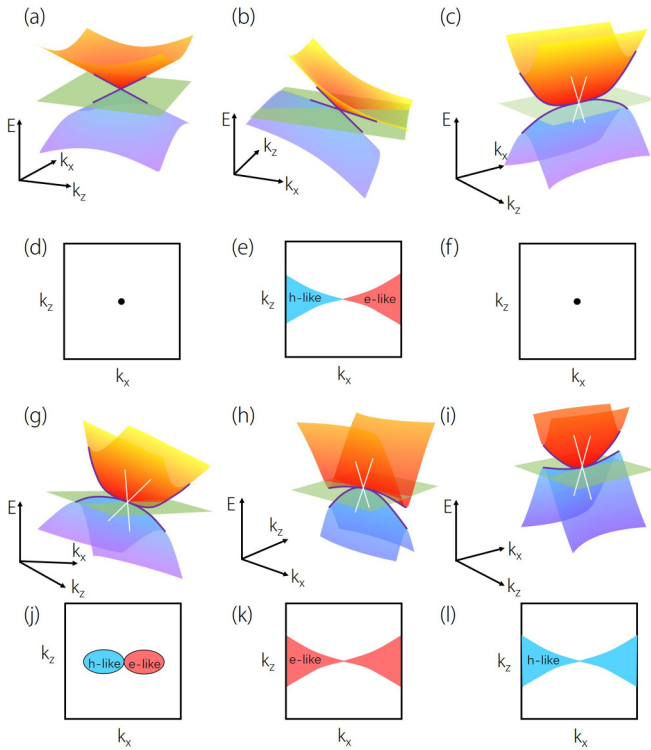


FIG. 1. (a)–(c) and (g)–(i) Three-dimensional plots of the phonon band dispersions around the WP in the k_x - k_z plane. The white and blue lines indicate the phonon dispersions along the k_z and k_x directions, respectively. (d)–(f) and (j)–(l) Constant-frequency contours in the k_x - k_z plane at the frequency of WPs. The blue and red regions in (e), (j), (k), and (l) represent the hole-like (h-like) and electron-like (e-like) states, respectively.

cannot be maintained when the spin-orbit coupling (SOC) is considered. In the case of $X_2\text{RhF}_6$, although the type-III C-2 WPs appear when the SOC is considered, the double-helicoid surface states are hidden by bulk band structures. Hence, it is still important to search for realistic materials with ideal type-III C-2 WPs and clean double-helicoid surface states.

C-1, C-2, and C-4 WP research has recently been extended from electronic systems to spinless phonon systems [27–35,35,36]. For example, WC-type materials [27], CdTe [28] and ZnSe [29], have been predicted to host C-1 Weyl point phonons (WPPs). α -SiO₂ [30], Rb₂Be₂O₃ [31], and K₂Sn₂O₃ [32] have been reported to host C-2 WPPs. BiIrSe and Li₃CuS₂ [33] are the hosts of C-4 WPPs. Phonons are bosons that are unaffected by the SOC effect and are not limited by the Fermi level. Thus, in principle, C-2 WPs can be found in all phonon dispersions. Moreover, topological phonons [37–41] can be used to investigate heat transfer, phonon scattering, and electron-phonon interactions. For example, a series of noncentrosymmetric materials with C-2 WPs in their phonon dispersions was reported using the first-principles calculations [34]. The experimental confirmation of C-2 WPPs in one of the noncentrosymmetric materials (FeSi) using inelastic x-ray scattering is encouraging [35]. Moreover, Wang *et al.* [30] and Huang *et al.* [36] proposed a symmetry-protected topological triangular Weyl complex formed by a C-2 WP and two C-1 WPs in the phonon dispersions of

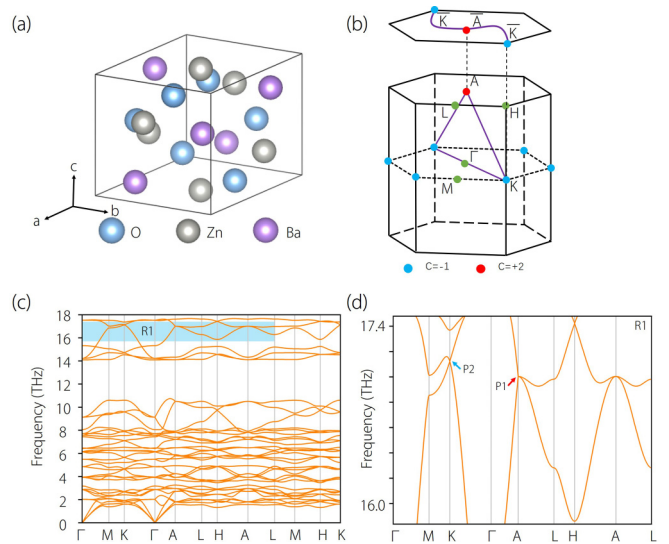


FIG. 2. (a) Crystal structure of BaZnO₂. (b) Three-dimensional BZ and projected (001) surface BZ. The red and blue dots represent the C-2 WP and C-1 WPs, respectively. The purple lines indicate the triangular Weyl complex. The projections of the WPs on the (001) surface are connected via visible double-helicoid surface states. (c) The phonon dispersion along the Γ -M-K- Γ -A-L-H-A-L-M-H-K paths and (d) the enlarged phonon dispersion of the phonon bands in the R1 region.

α -SiO₂ and SrSi₂. However, to date, all the proposed C-2 WPs in phonon systems [30,34–36] have type-I phonon band dispersion [see Fig. 1(c)]. Thus, it is only natural to ask whether type-III C-2 WPPs exist in a realistic three-dimensional crystal. This question is certainly answered in this paper.

Herein, based on first-principles calculations and symmetry analysis, we propose a realistic material (BaZnO₂) [42] with space group $P3_121$ and a type-III C-2 WPP at a high-symmetry point (HSP). Note that BaZnO₂ is an excellent platform for realizing type-III C-2 WPPs for the following reasons: (i) The frequency region (named R1) of the type-III C-2 WP is very clean, and the phonon bands that form the type-III C-2 WP do not overlap with other phonon branches in region R1. (ii) The presence of visible double-helicoid surface states connected to the projection of the type-III C-2 WP aids experimental detection. (iii) BaZnO₂ has two type-I C-1 WPs at HSPs in addition to the type-III C-2 WP at HSP A. That is, the WPs in BaZnO₂ do not appear in pairs with opposite chiral charges and can therefore form a particular triangular Weyl complex. Although Wang *et al.* [30] first proposed the triangular Weyl complex in SiO₂ phonons, the C-2 WP in SiO₂ phonons is type-I and is different from the type-III C-2 WP in BaZnO₂ phonons. We propose a type-III C-2 WP-based triangular Weyl complex in a phonon system.

II. COMPUTATIONAL METHODS AND MATERIAL

BaZnO₂ [42] can be prepared by heating BaCO₃ and ZnO mixtures in a high vacuum at temperatures up to 1100 °C. Figure 2(a) depicts the crystal structure of BaZnO₂ with space group $P3_121$. We carried out first-principles calculations as implemented in the Vienna Ab initio Simulation

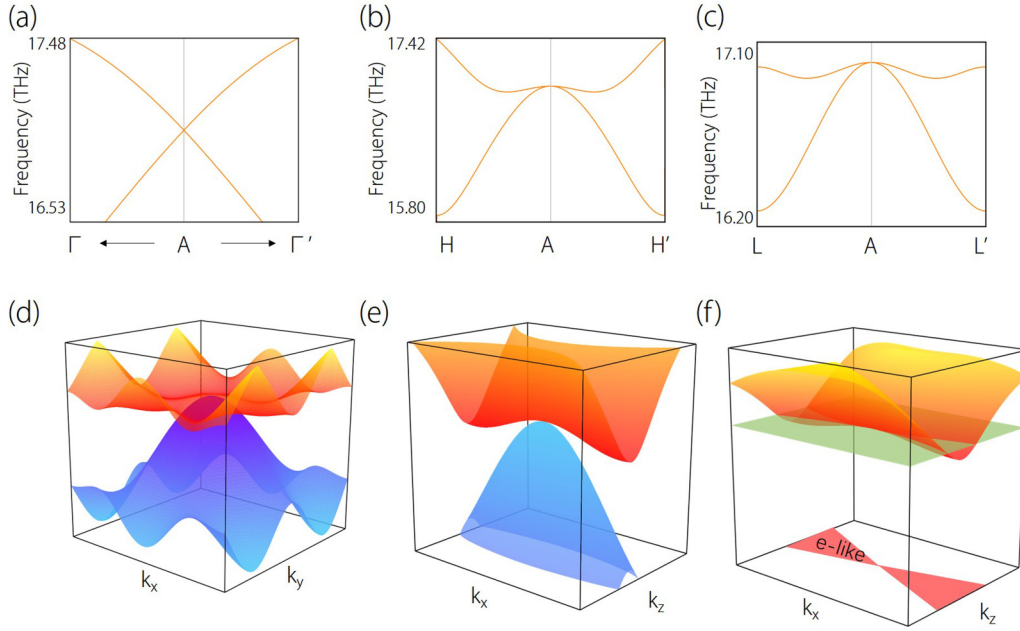


FIG. 3. (a)–(c) Phonon dispersions along Γ - A - Γ' , H - A - H' , and L - A - L' , respectively. (d) and (e) Three-dimensional plots of the phonon band dispersions around the C-2 WP in the k_x - k_y and k_x - k_z planes, respectively. (f) Constant-frequency surface of the C-2 WP (P1), which contains two connected e-like states. The green surface in (f) represents the constant-frequency surface at P1.

Package (VASP) code [43] to obtain the ground state of BaZnO_2 within the framework of the density-functional theory (DFT). The exchange-correlation potential was determined using the generalized gradient approximation [44] of the Perdew-Burke-Ernzerhof type. The interactions between ions and valence electrons were investigated using the projector augmented-wave [45] method, with an energy cutoff of 520 eV. A Γ -centered k mesh of $6 \times 6 \times 5$ was used for BZ sampling. The convergence condition of the electronic self-consistent loop was set to 10^{-6} eV. The crystal structure was totally relaxed until the maximum force on each atom was less than -0.01 eV/Å. The obtained lattice constants from the first-principles calculations are $a = b = 5.96$ Å and $c = 6.82$ Å, which are in good agreement with the experimental values ($a = b = 5.82$ Å and $c = 6.73$ Å). The Ba, Zn, and O atoms in the relaxed crystal structure are located at the 3b, 3a, and 6c Wyckoff sites, respectively. To study the phonon dispersion of BaZnO_2 , we built a $2 \times 2 \times 2$ supercell and used the PHONOPY package [46] within the density-functional perturbation theory to perform lattice dynamic calculations for the supercell. The surface states of the phonons were simulated using the following steps: First, we used the PHONOPYTB tool [47], which was installed in the root folder of WANNIERTOOLS [48], to generate the phononic tight-binding Hamiltonian with the FORCE-CONSTANTS. Thereafter, we used the iterative Green's function method [49] to calculate the surface states of the phonons in the WANNIERTOOLS software package.

III. TYPE-III C-2 WPP IN BAZNO₂

Figure 2(c) shows the calculated phonon dispersion of BaZnO_2 along the Γ - M - K - Γ - A - L - H - A - L - M - H - K paths [see Fig. 2(b)]. The material is found to be free of unstable

vibrational modes in its phonon dispersion, indicating that it is dynamically stable. As shown in Fig. 2(c), the phonon dispersion curves in R1 are important because the optical phonon branches in R1 are very clean. There are several notable features in the close-up [see Fig. 2(d)]: (i) Two points have twofold degeneracy. These two WPs (P1 and P2) are located at HSPs A and K, respectively, and they are derived from the two phonon branches (with numbers 34 and 35). (ii) The phonon dispersion around HSP K is linear, whereas the phonon dispersion around HSP A is not.

As shown in Figs. 3(a)–3(c), the phonon dispersions around HSP A along the k_z axis are linear. However, the phonon dispersions at HSP A along the k_y and k_x axes are quadratic. Actually, a quadratic phonon band splitting around HSP A can be found in the whole k_y - k_x plane normal to the k_z direction [see Fig. 3(d)]. The Chern number of P1 on a sphere enclosing the Weyl node was determined by tracing the evolution of the average position of the Wannier centers using the Wilson loop approach [48]. Figure 4(a) shows the results, which reveal that P1 has a Chern number of 2, indicating that it is a C-2 WP.

The C-2 WP at HSP A is symmetry dominated. Hence, we performed symmetry analysis to further understand the occurrence of the C-2 WP in space group $P3_121$. We discovered that the crossing point at A around 17 THz is formed by a two-dimensional corepresentation, A_3 , of space group 152 [50,51]. The corepresentation matrices of A_3 can be expressed as

$$C_3^+ = e^{i\pi\sigma_z/3}, C_{21}'' = \sigma_y, \mathcal{T} = i\sigma_x. \quad (1)$$

Thus, the $\mathbf{k} \cdot \mathbf{p}$ Hamiltonian of A_3 can be written (up to second order) under the symmetry constraints as

$$H = \varepsilon + \omega_{\parallel} k_{\parallel}^2 + \omega_z k_z \sigma_z + [i(ak_-^2 + bk_+ k_+) \sigma_+ + \text{H.c.}], \quad (2)$$

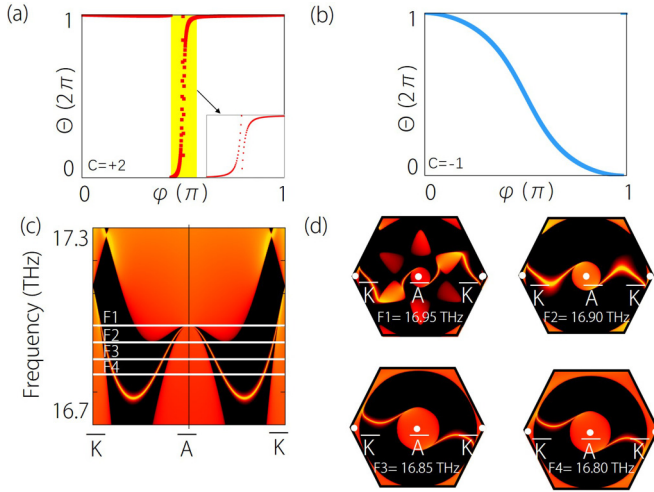


FIG. 4. The evolution of the average position of the Wannier centers for the P1 WP with positive chirality. (b) The evolution of the average position of the Wannier centers for the P2 WP with negative chirality. (c) The phonon LDOS of BaZnO₂ along the \bar{K} - \bar{A} - \bar{K} surface paths on the (001) surface. (d) Frequency slice for BaZnO₂ corresponding to the (001) surface at different frequencies.

where ε , ω , a , and b are real parameters, σ_i ($i = x, y, z$) are Pauli matrices, $k_{\parallel}^2 = k_x^2 + k_y^2$, $k_{\pm} = k_x \pm ik_y$, and $\sigma_{\pm} = \sigma_x \pm i\sigma_y$. The leading order of such a Hamiltonian is (122), indicating that this point is a C-2 WP [20].

Figure 3(e) shows the three-dimensional plots of the phonon dispersion around the C-2 WP at HSP A in the k_x - k_z plane. The dispersion shape resembles a saddle, as shown in Fig. 1(h). The WP shown in Fig. 3(e) is a type-III WP, and there are two connected e-like states in the constant-frequency surface at P1 [see Fig. 3(f)].

To better understand why the C-2 WP at HSP A has a type-III dispersion, we present a detailed symmetry analysis as follows. It is worth noting that the band dispersion for the $k_z = 0$ plane can be simply written as $E_{\pm}(\mathbf{k}) = (\omega_{\parallel} \pm a)k_{\parallel}^2$. When the quadratic tilting term, $\omega_{\parallel}k_{\parallel}^2$, dominates the energy dispersion, i.e., $|\omega_{\parallel}| > |a|$, a type-III WP is produced [26]. To further confirm our results, we fitted the phonon band structure with the DFT results for the C-2 WP (see Fig. S1 in the Supplemental Material (SM) [52]). For this material, we have $|\omega_{\parallel}| > |a|$, indicating that the crossing point at A is a type-III WP.

IV. TYPE-III C-2 WP-BASED TRIANGULAR WEYL COMPLEX PHONONS IN BAZNO2

As shown in Fig. 2(d), another WP named P2 exists at HSP K. As shown in Fig. 4(b), the WP at point K between phonon branches 34 and 35 is a C-1 WP because the Chern number of P2 is -1 . The C-1 WP at HSP K exhibits a linear energy splitting along any direction in momentum space [28,53] (see Fig. 5), and it has a pointlike frequency surface [54]. Hence, the C-1 WP at HSP K is a type-I WP, as shown in Fig. 1(a).

The following is a detailed symmetry analysis of the type-I C-1 WPs of BaZnO₂ at two K HSPs. The crossing point at K around 17 THz is formed by a two-dimensional corepresentation, K_3 , of space group 152 [50,51]. The corepresentation

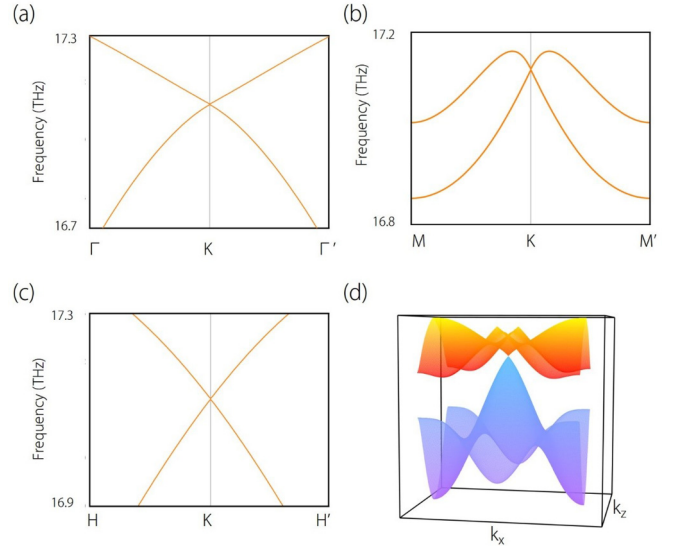


FIG. 5. (a)–(c) Phonon dispersions along the Γ - K - Γ' , M - K - M' , and H - K - H' paths, respectively (d) Three-dimensional plot of the phonon band dispersion around the C-1 WP (P2) in the k_x - k_z plane.

matrices of K_3 can be expressed as

$$C_3^+ = e^{-2i\pi\sigma_y/3}, \quad C_{21}'' = \sigma_z. \quad (3)$$

Then the $\mathbf{k} \cdot \mathbf{p}$ Hamiltonian of K_3 can be written as

$$\varepsilon + c_1\sigma_x k_x + c_2\sigma_z k_y + c_3\sigma_y k_z, \quad (4)$$

which is a standard C-1 WP [55]. There is no tilted term in such a Hamiltonian, and the band dispersion around the K point is $E_{\pm}(\mathbf{k}) = \varepsilon \pm \sqrt{c_1^2 k_x^2 + c_2^2 k_y^2 + c_3^2 k_z^2}$. Therefore, we always have $E_{\pm}(\mathbf{k}) = E_{\pm}(-\mathbf{k})$, giving rise to a type-I WP at K point.

Note that there are six K points in the first BZ, and each K point is shared by three neighboring Wigner-Seitz cells in momentum space. Interestingly, the type-III C-2 WP has a chiral charge of $+2$, and the two type-I C-1 WPs have a total chiral charge of -2 , resulting in a zero total chiral charge. Hence, the C-2 WP and the two C-1 WPs can form a symmetry-dominated triangular Weyl complex, as shown in Fig. 2(b).

We would like to highlight the following points: (i) The triangular Weyl complex proposed herein contains a type-III C-2 WP, which is different from the triangular Weyl complex proposed by Wang *et al.* [30] and Huang *et al.* [36]. The C-2 WPs mentioned in both of those papers are all type-I C-2 WPs [see Fig. 1(c)], which have no saddlelike dispersion. (ii) Electronic systems have been the only focus of the search for type-III WPs [25,26] up to now. Type-III C-2 WPs must be close to the Fermi level to be detectable or manifest physical properties in electronic systems. There is no notion of Fermi level for phonons [56–58]. Therefore, type-III C-2 WPs may exist much more universally in phonon systems than in electronic systems. (iii) Type-I C-2 WPs in FeSi phonons [35] have already been experimentally confirmed using inelastic x-ray scattering, providing a strong driving force for the search for the C-2 WP in phonons. Future research should explore other types of C-2 WPs (such as type-III C-2 WPs) in phonons

TABLE I. The crystal systems that can host C-2 WPPs at HSPs. IRR is the irreducible (co)representation of the WPPs. Here, the material candidates with type-III C-2 WPPs are given.

Crystal systems	SGs (HSPs)	IRR	Materials
Tetragonal	75 (Γ, M, A, Z), 76 (Γ, M), 77 (Γ, M, A, Z), 78 (Γ, M), 79 (Γ, Z, P), 80 (Γ, Z)	$\{R_2, R_4\}$	Mg_2TiO_4 [SG 91]
	89 (Γ, M, A, Z), 90 (Γ, Z), 91 (Γ, M), 92 (Γ), 93 (Γ, M, A, Z), 94 (Γ, Z), 95 (Γ, M), 96 (Γ), 97 (Γ, Z, P), 98 (Γ, Z)	R_5	
Trigonal	143–145 (Γ, A), 146 (Γ, Z)	$\{R_2, R_3\}$	Li_2GeF_6 [SG 154]
	149–154 (Γ, A), 155 (Γ, Z)	R_3	
Hexagonal	168 (Γ, A), 169–170 (Γ), 171–172 (Γ, A), 173 (Γ)	$\{R_2, R_6\}$ or $\{R_3, R_5\}$	CaSO_4 [SG 180]
	177 (Γ, A), 178–179 (Γ), 180–181 (Γ, A), 182 (Γ)	R_5 or R_6	
Cubic	196 (L),	$\{R_2, R_3\}$	$\text{Li}_{10}\text{B}_{14}\text{Cl}_2\text{O}_{25}$ [SG 196]
	207–208 (X, M)	R_5	
	209 (X, L, W), 210 (X, L)	$X: R_5; L: R_3; W: \{R_3, R_4\}$	
Triclinic			
Orthorhombic			
Monoclinic			

and investigate their related physical properties theoretically and experimentally.

V. VISIBLE DOUBLE-HELICOID PHONONIC SURFACES IN BaZnO_2

A vital feature of the WP in phonons is the presence of arc-shaped phononic surface states [29,30,33,34,36]. In Fig. 2(b), we projected the A and K symmetry points in the bulk BZ to the \bar{A} and \bar{K} points on the (001) surface. Figure 4(c) shows the phonon local density of states (LDOS) projected on the (001) surface of BaZnO_2 . There are two prominent surface states, starting from the \bar{A} point and ending at the two \bar{K} points. Figure 4(d) also shows the constant frequency slices corresponding to the (001) surface at $F1 = 16.95$ THz, $F2 = 16.90$ THz, $F3 = 16.85$ THz, and $F4 = 16.80$ THz. In Fig. 4(d), two surface arcs wind counterclockwise around the \bar{A} point, and the projection of the C-2 WP can be viewed as a double-helicoid because its Chern number is equal to 2. More importantly, we would like to emphasize that the double-helicoid surface states in BaZnO_2 are both clean and long. The double-helicoid surface states can span the entire first surface BZ [see Fig. 2(b) for the schematic diagram and Fig. 4(d) for the results]. The clear and long surface states can greatly promote their detection in future experiments.

VI. ADDITIONAL NOTES

Before closing, we added three additional notes as follows:

(i) Note that the C-2 WPPs are symmetry dominated. To support the inspiring findings of the C-2 WPPs, via symmetry analysis, we go through the 230 type-II magnetic space groups (SGs) [20] to screen out the ones that can exhibit C-2 WPPs at a certain frequency range at HSPs. The results are given in Table I. We find that the C-2 WPPs may appear at HSPs of some tetragonal, trigonal, hexagonal, and cubic-type crystals. However, we cannot find the C-2 WPPs at HSPs in the triclinic, rhombohedral, and monoclinic crystals.

(ii) Although the C-2 WPPs at HSPs can be determined by symmetry, the type of band dispersion cannot be directly

determined by the symmetry analysis. Nevertheless, we can narrow down the search range for type-III C-2 WPPs at HSPs based on Table I. That is, we can further search for C-2 WPPs at HSPs with type-III band dispersion among the candidate SGs, i.e., 75–80, 89–98, 143–146, 149–155, 168–173, 177–182, 196, and 207–210. As typical examples, in Table I, we show four materials, i.e., tetragonal Mg_2TiO_4 , trigonal Li_2GeF_6 , hexagonal CaSO_4 , and cubic $\text{Li}_{10}\text{B}_{14}\text{Cl}_2\text{O}_{25}$, host type-III C-2 WPPs at HSPs. More details about the crystal structures and the phonon dispersions are given in Figs. S2–S5 (see the SM [52]). For example, as shown in Fig. S5 (see SM [52]), we can find a type-III C-2 WP at the L HSP in the phonon dispersion of the cubic $\text{Li}_{10}\text{B}_{14}\text{Cl}_2\text{O}_{25}$, which agrees with the data shown in Table I.

(iii) Moreover, it is reasonable to expect that type-III C-2 WPPs can induce novel physical properties according to the saddlelike dispersion and topological charge. Besides phonons, our investigation also guides exploring type-III C-2 Weyl points in artificial systems such as acoustic crystals.

VII. SUMMARY

In summary, based on first-principles calculations, we proposed that BaZnO_2 with space group $P3_121$ hosts a type-III C-2 WP in its phonon dispersion. It is worth noting that no research has addressed type-III WPPs, which have a constant-frequency surface that consists of two connected e-like or h-like states. The type-III WPP in BaZnO_2 is very clean, and the phonon bands that form the WP do not overlap with other phonon bands in a certain region called R1, which guarantees that it would be readily detectable in experiments. More importantly, the type-III C-2 WP and two type-I C-1 WPs can form a triangular Weyl complex. Although researchers have proposed certain triangular Weyl complexes in realistic materials, they are all formed by type-I WPs. The double-helicoid surfaces that connect the projections of the type-III C-2 WP and two type-I C-1 WPs are very visible, clean, and lengthy on the (001) surface.

Moreover, we pointed out that type-III C-2 WPPs may appear at HSPs in SGs 75–80, 89–98, 143–146,

149–155, 168–173, 177–182, 196, and 207–210. Some material candidates, including tetragonal MgTiO_4 , trigonal Li_2GeF_6 , hexagonal CaSO_4 , and cubic $\text{Li}_{10}\text{B}_{14}\text{Cl}_2\text{O}_{25}$, are also proposed to be hosts of type-III C-2 WPPs. Our findings can be viewed as a guide for further investigation of type-III C-2 WPPs.

ACKNOWLEDGMENTS

Z.Z. is grateful for the support from the National Natural Science Foundation of China (Grant No. 12004028). X.W. is grateful for the support from the National Natural Science Foundation of China (Grant No. 51801163).

-
- [1] B. Yan and C. Felser, *Annu. Rev. Condens. Matter Phys.* **8**, 337 (2017).
- [2] P. Hosur and X. Qi, *C. R. Phys.* **14**, 857 (2013).
- [3] A. A. Soluyanov, D. Gresch, Z. Wang, Q. Wu, M. Troyer, X. Dai, and B. A. Bernevig, *Nature (London)* **527**, 495 (2015).
- [4] P. G. LaBarre, L. Dong, J. Trinh, T. Siegrist, and A. P. Ramirez, *J. Phys.: Condens. Matter* **32**, 02LT01 (2019).
- [5] Y. Sun, S.-C. Wu, and B. Yan, *Phys. Rev. B* **92**, 115428 (2015).
- [6] B. Q. Lv, H. M. Weng, B. B. Fu, X. P. Wang, H. Miao, J. Ma, P. Richard, X. C. Huang, L. X. Zhao, G. F. Chen, Z. Fang, X. Dai, T. Qian, and H. Ding, *Phys. Rev. X* **5**, 031013 (2015).
- [7] Y. Sun, Y. Zhang, C. Felser, and B. Yan, *Phys. Rev. Lett.* **117**, 146403 (2016).
- [8] G. Chang, S.-Y. Xu, H. Zheng, C.-C. Lee, S.-M. Huang, I. Belopolski, D. S. Sanchez, G. Bian, N. Alidoust, T.-R. Chang, C.-H. Hsu, H.-T. Jeng, A. Bansil, H. Lin, and M. Z. Hasan, *Phys. Rev. Lett.* **116**, 066601 (2016).
- [9] G. Xu, H. Weng, Z. Wang, X. Dai, and Z. Fang, *Phys. Rev. Lett.* **107**, 186806 (2011).
- [10] D. Bulmash, C.-X. Liu, and X.-L. Qi, *Phys. Rev. B* **89**, 081106(R) (2014).
- [11] T. Ojanen, *Phys. Rev. B* **87**, 245112 (2013).
- [12] Y. Okamura, S. Minami, Y. Kato, Y. Fujishiro, Y. Kaneko, J. Ikeda, J. Muramoto, R. Kaneko, K. Ueda, V. Kocsis, N. Kanazawa, Y. Taguchi, T. Koretsune, K. Fujiwara, A. Tsukazaki, R. Arita, Y. Tokura, and Y. Takahashi, *Nat. Commun.* **11**, 4619 (2020).
- [13] X. Huang, L. Zhao, Y. Long, P. Wang, D. Chen, Z. Yang, H. Liang, M. Xue, H. Weng, Z. Fang, X. Dai, and G. Chen, *Phys. Rev. X* **5**, 031023 (2015).
- [14] A. A. Burkov, *Phys. Rev. Lett.* **113**, 187202 (2014).
- [15] J. F. Steiner, A. V. Andreev, and D. A. Pesin, *Phys. Rev. Lett.* **119**, 036601 (2017).
- [16] T. Higo, D. Qu, Y. Li, C. L. Chien, Y. Otani, and S. Nakatsuji, *Appl. Phys. Lett.* **113**, 202402 (2018).
- [17] B. Bradlyn, J. Cano, Z. Wang, M. G. Vergniory, C. Felser, R. J. Cava, and B. A. Bernevig, *Science* **353**, 6299 (2016).
- [18] S.-M. Huang, S.-Y. Xu, I. Belopolski, C.-C. Lee, G. Chang, T.-R. Chang, B. Wang, N. Alidoust, G. Bian, M. Neupane, D. Sanchez, H. Zheng, H.-T. Jeng, A. Bansil, T. Neupert, H. Lin, and M. Z. Hasan, *Proc. Natl. Acad. Sci. U.S.A.* **113**, 1180 (2016).
- [19] T. T. Zhang, R. Takahashi, C. Fang, and S. Murakami, *Phys. Rev. B* **102**, 125148 (2020).
- [20] Z.-M. Yu, Z. Zhang, G.-B. Liu, W. Wu, X.-P. Li, R.-W. Zhang, S. A. Yang, and Y. Yao, *Sci. Bull.* **67**, 375 (2022).
- [21] C. Cui, X. P. Li, D. S. Ma, Z. M. Yu, and Y. Yao, *Phys. Rev. B* **104**, 075115 (2021).
- [22] W. Z. Meng, X. M. Zhang, T. L. He, L. Jin, X. F. Dai, Y. Liu, and G. D. Liu, *J. Adv. Res.* **24**, 523 (2020).
- [23] S. Borisenko, D. Evtushinsky, Q. Gibson, A. Yaresko, K. Koepernik, T. Kim, M. Ali, J. van den Brink, M. Hoesch, A. Fedorov, E. Haubold, Y. Kushnirenko, I. Soldatov, R. Schafer, and R. J. Cava, *Nat. Commun.* **10**, 3424 (2019).
- [24] M.-Y. Yao, N. Xu, Q. S. Wu, G. Autès, N. Kumar, V. N. Strocov, N. C. Plumb, M. Radovic, O. V. Yazyev, C. Felser, J. Mesot, and M. Shi, *Phys. Rev. Lett.* **122**, 176402 (2019).
- [25] L. Jin, X. Zhang, Y. Liu, X. Dai, L. Wang, and G. Liu, *Phys. Rev. B* **102**, 195104 (2020).
- [26] X.-P. Li, K. Deng, B. Fu, Y. Li, DaShuai Ma, J. F. Han, J. Zhou, S. Zhou, and Y. Yao, *Phys. Rev. B* **103**, L081402 (2021).
- [27] Q. Xie, J. X. Li, S. Ullah, R. H. Li, L. Wang, D. Z. Li, Y. Y. Li, S. Yunoki, and X.-Q. Chen, *Phys. Rev. B* **99**, 174306 (2019).
- [28] B. W. Xia, R. Wang, Z. J. Chen, Y. J. Zhao, and H. Xu, *Phys. Rev. Lett.* **123**, 065501 (2019).
- [29] P. F. Liu, J. Li, X. H. Tu, H. Li, J. Zhang, P. Zhang, Q. Gao, and B. T. Wang, *Phys. Rev. B* **103**, 094306 (2021).
- [30] R. Wang, B. W. Xia, Z. J. Chen, B. B. Zheng, Y. J. Zhao, and H. Xu, *Phys. Rev. Lett.* **124**, 105303 (2020).
- [31] Y. J. Jin, Z. J. Chen, X. L. Xiao, and H. Xu, *Phys. Rev. B* **103**, 104101 (2021).
- [32] Q.-B. Liu, Y. Qian, H.-H. Fu, and Z. Wang, *npj Comput. Mater.* **6**, 95 (2020).
- [33] Q.-B. Liu, Z. Wang, and H.-H. Fu, *Phys. Rev. B* **103**, L161303 (2021).
- [34] T. Zhang, Z. Song, A. Alexandradinata, H. Weng, C. Fang, L. Lu, and Z. Fang, *Phys. Rev. Lett.* **120**, 016401 (2018).
- [35] H. Miao, T. T. Zhang, L. Wang, D. Meyers, A. H. Said, Y. L. Wang, Y. G. Shi, H. M. Weng, Z. Fang, and M. P. M. Dean, *Phys. Rev. Lett.* **121**, 035302 (2018).
- [36] Z. Huang, Z. Chen, B. Zheng, and H. Xu, *npj Comput. Mater.* **6**, 87 (2020).
- [37] J. Li, L. Wang, J. Liu, R. Li, Z. Zhang, and X.-Q. Chen, *Phys. Rev. B* **101**, 081403(R) (2020).
- [38] S. Singh, Q. S. Wu, C. Yue, A. H. Romero, and A. A. Soluyanov, *Phys. Rev. Materials* **2**, 114204 (2018).
- [39] Y. Liu, X. Chen, and Y. Xu, *Adv. Funct. Mater.* **30**, 1904784 (2020).
- [40] J. Li, J. Liu, S. A. Baronett, M. Liu, L. Wang, R. Li, Y. Chen, D. Li, Q. Zhu, and X. Chen, *Nat. Commun.* **12**, 1204 (2020).
- [41] X.-Q. Chen, J. Liu, and J. Li, *Innovation* **2**, 100134 (2021).
- [42] U. Spitsbergen, *Acta Crystallogr.* **13**, 197 (1960).
- [43] J. Hafner, *J. Comput. Chem.* **29**, 2044 (2008).
- [44] J. P. Perdew, K. Burke, and M. Ernzerhof, *Phys. Rev. Lett.* **77**, 3865 (1996).
- [45] P. E. Blöchl, *Phys. Rev. B* **50**, 17953 (1994).
- [46] A. Togo and I. Tanaka, *Scr. Mater.* **108**, 1 (2015).

- [47] https://github.com/quanshengwu/wannier_tools/tree/master/utility/phonopyTB.
- [48] Q. S. Wu, S. N. Zhang, H.-F. Song, M. Troyer, and A. A. Soluyanov, *Comput. Phys. Commun.* **224**, 405 (2018).
- [49] F. Guinea, C. Tejedor, F. Flores, and E. Louis, *Phys. Rev. B* **28**, 4397 (1983).
- [50] G. B. Liu, M. Chu, Z. Zhang, Z. M. Yu, and Y. Yao, *Comput. Phys. Commun.* **265**, 107993 (2021).
- [51] C. Bradley and A. Cracknell, *The Mathematical Theory of Symmetry in Solids: Representation Theory for Point Groups and Space Groups* (Oxford University Press, Oxford, 2009).
- [52] See Supplemental Material at <http://link.aps.org/supplemental/10.1103/PhysRevB.105.134303> for a comparison of the $\mathbf{k} \cdot \mathbf{p}$ Hamiltonian (solid line), crystal structures, three-dimensional BZ, calculated phonon dispersions, and enlarged phonon bands around the type-III C-2 WPPs in tetragonal MgTiO_4 , trigonal Li_2GeF_6 , hexagonal CaSO_4 , and cubic $\text{Li}_{10}\text{B}_{14}\text{Cl}_2\text{O}_{25}$.
- [53] J. Liu, W. Hou, E. Wang, S. Zhang, J.-T. Sun, and S. Meng, *Phys. Rev. B* **100**, 081204(R) (2019).
- [54] J. Li, Q. Xie, S. Ullah, R. Li, H. Ma, D. Li, Y. Li, and X.-Q. Chen, *Phys. Rev. B* **97**, 054305 (2018).
- [55] X. Wan, A. M. Turner, A. Vishwanath, and S. Y. Savrasov, *Phys. Rev. B* **83**, 205101 (2011).
- [56] J.-Y. You, X.-L. Sheng, and G. Su, *Phys. Rev. B* **103**, 165143 (2021).
- [57] H. Chen, W. Wu, J. Zhu, S. A. Yang, and L. Zhang, *Nano Lett.* **21**, 3060 (2021).
- [58] Z. J. Chen, R. Wang, B. W. Xia, B. B. Zheng, Y. J. Jin, Y. J. Zhao, and H. Xu, *Phys. Rev. Lett.* **126**, 185301 (2021).